Inorganic Chemistry

Article

pubs.acs.org/IC

Magnetic Properties of 1:2 Mixed Cobalt(II) Salicylaldehyde Schiff-Base Complexes with Pyridine Ligands Carrying High-Spin Carbenes (S_{car} = 2/2, 4/2, 6/2, and 8/2) in Dilute Frozen Solutions: Role of Organic Spin in Heterospin Single-Molecule Magnets

Satoru Karasawa,[†] Kimihiro Nakano,[†] Daisuke Yoshihara,[†] Noriko Yamamoto,[†] Jun-ichi Tanokashira,[†] Takahito Yoshizaki,[†] Yuji Inagaki,[‡] and Noboru Koga*[,†]

[†]Graduate School of Pharmaceutical Sciences, Kyushu University, 3-1-1 Maidashi, Higashi-ku, Fukuoka, 812-8582 Japan

[‡]Department of Applied Quantum Physics, Kyushu University, 744 Motooka, Nishi-ku, Fukuoka, 812-0395 Japan

Supporting Information

ABSTRACT: The 1:2 mixtures of Co(*p*-tolsal)$_2$, *p*-tolsal = *N*-*p*-tolylsalicylideniminato, and diazo-pyridine ligands, **DXpy**; **X** = **1**, **2**, **3l**, **3b**, and **4**, in MTHF solutions were irradiated at cryogenic temperature to form the corresponding 1:2 cobalt−carbene complexes Co(*p*-tolsal)$_2$(**CXpy**)$_2$, with S_{total} = 5/2, 9/2, 13/2, 13/2, and 17/2, respectively. The resulting Co(*p*-tolsal)$_2$(**CXpy**)$_2$, **X** = **1**, **2**, **3l**, **3b**, and **4**, showed magnetic behaviors characteristic of heterospin single-molecule magnets with effective activation barriers, U_{eff}/k_B, of 40, 65, 73, 72, and 74 K, for reorientation of the magnetic moment and temperature-dependent hysteresis loops with a coercive force, H_c, of ∼0, 6.2, 10, 6.5, and 9.0 kOe at 1.9 K, respectively. The relaxation times, τ_Q, due to a quantum tunneling of magnetization (QTM) were estimated to be 1.6 s for Co(*p*-tolsal)$_2$(**C1py**)$_2$, ∼2.0 × 10^3 s for Co(*p*-tolsal)$_2$(**C2py**)$_2$, and >10^5 s for Co(*p*-tolsal)$_2$(**CXpy**)$_2$; **X** = **3b**, **3l**, and **4**. In heterospin complexes, organic spins, carbenes interacted with the cobalt ion to suppress the QTM pathway, and the τ_Q value increased with increasing the S_{total} values.

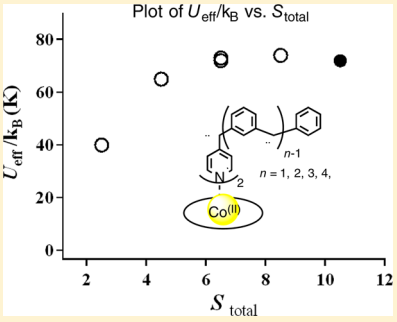

INTRODUCTION

Single-molecule magnets (SMMs)[1−6] exhibiting hysteresis loops of magnetization similar to bulk magnets and the spin quantum tunneling effect at low temperatures have been attracting the interest of many chemists in the fields of both new functional materials and fundamental chemistry. In an SMM, the characteristic slow magnetic relaxation for reorientation of the magnetic moment takes place via various pathways due to the direct,[1a,7] Orbach,[1a,7] Raman,[1a,7] and quantum tunneling of the magnetization (QTM)[2−6] process. The thermodynamic activation barrier, U/k_B, corresponds to $|D|S^2$ and $|D|(S^2 - 1/4)$ for integer spin and noninteger spin, respectively, where $|D|$ ($D < 0$) is a uniaxial anisotropic parameter and S is a spin quantum number. Therefore, the effective activation barriers (U_{eff}/k_B: $U_{eff}/k_B < U/k_B$) depend on the U/k_B value and the relaxation pathways, especially QTM relaxation time, τ_Q. To obtain a large U_{eff}/k_B in SMMs, an increasing U/k_B value and/or a suppressing QTM pathway would be required.

For the construction of SMMs, we used a heterospin system[8,9] consisting of the 3d spins of the anisotropic metal ions and the 2p spins of the organic spins. In our heterospin systems, carbene[9b,d−f] and a stable aminoxyl[9a,c] were used as organic spins, and they magnetically interacted with 3d metal ions through aromatic ligands by the large delocalization of π-spin of organic unpaired electrons. Recently, other groups also reported heterospin SMMs taking advantage of the magnetic coupling between the anisotropic metal ion and organic radicals.[10] In our heterospin systems, the combination of a high-spin cobalt(II) ion and the pyridine-carbene[11] and -aminoxyl[11e,12] ligands provided unique heterospin SMMs having slow magnetic relaxation with a large U_{eff}/k_B and showing the hysteresis loop of magnetization, M, with a large coercive force (H_c) above 1.9 K. The values of U_{eff}/k_B and H_c at 1.9 K for heterospin SMMs, especially cobalt−carbene complexes, were considerably large compared with those for metal clusters containing 3d metals reported as SMMs up to now. The schematic structures designed according to the strategy of our heterospin SMM are shown in Scheme 1. Notably, the monometallic 1:4 cobalt complexes Co(NCO)$_2$(**C1py**)$_4$[11a,b,e−g] and the cyclic 2:2 cobalt complexes[11c,d] [Co(I-hfpip)$_2$(**C2py$_2$**)]$_2$, I-hfpip = 1,1,1,5,5,5-hexafluoro-4-(4-iodophenylimino)-2-pentanonate, showed SMM behaviors with extra large values of U_{eff}/k_B = 130 and 139 K and H_c = 20 and 26 kOe at 1.9 K, respectively, in addition to the temperature-independent QTM relaxation times (τ_Q) of 1.0 × 10^5 and 1.1 × 10^5 s, respectively.

The cobalt complexes for heterospin SMMs had similar compressed or elongated octahedral structures.[11a,b] In those

Received: December 15, 2013
Published: May 9, 2014

   dx.doi.org/10.1021/ic403074d | *Inorg. Chem.* 2014, 53, 5447−5457

Scheme 1. Schematic Structures of Heterospin SMMs

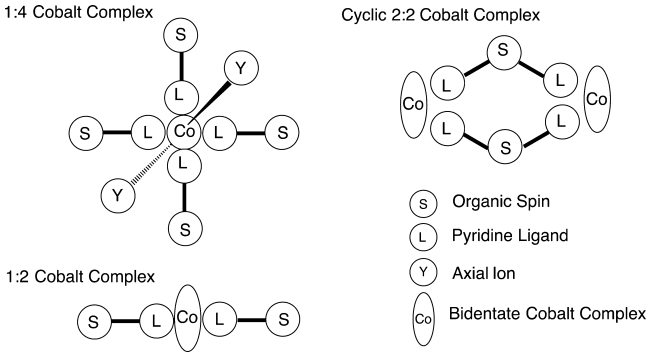

complexes, the z axis of the axial ligands might be anisotropic axes, and the organic spins were located in the $x-y$ plane of the cobalt complex. To understand heterospin SMMs, the effects of an axial ligand and organic spin (Y and S, respectively, in Scheme 1) in the cobalt complexes on the heterospin SMM property were systematically investigated in frozen solution. In the 1:4 cobalt−aminoxyl and −carbene complexes,[11b,12b,c] $Co(Y)_2$(**4NOpy**)$_4$ and $Co(Y)_2$(**C1py**)$_4$, Y = NCS^-, Cl^- (Br^- for **4NOpy** complex), and NCO^-, respectively, the axial ligand (ion) was revealed to strongly affect the U_{eff}/k_B (or U/k_B) for SMMs, and the U_{eff}/k_B values increased in the order Y = NCS^-, Cl^- (Br^-), and NCO^-. This result might be due to the increase of the $|D|$ value caused by the change of axial ligand. In the heterospin SMM, on the other hand, the role of organic spin located in the $x-y$ plane of the cobalt complex has not yet been sufficiently clarified. However, according to the experimental facts before irradiation, the diazo-Co complex showed no SMM behavior, while after irradiation, the carbene-Co complexes generated by photolysis of the diazo moieties showed SMM behavior, obviously indicating that the carbenes affected the SMM properties of carbene−Co complexes. Furthermore, since the U/k_B value of cobalt complexes corresponded to $|D|(S^2 - 1/4)$ for noninteger spin, the increase of the S value in the ground state by using triplet carbene spins would be expected to lead to a large U/k_B value. Recently, the 1:4 complexes of $CoCl_2$ and **DXpy**, **X** = **1**, **2**, **3l**, **3b**, and **4**, which were precursors of high-spin carbene−pyridine ligands with spin multiplicities, S_{car}, of 2/2, 4/2, 6/2, 6/2, and 8/2, respectively, were employed to change the S_{car} of carbenes systematically, and the influence of the carbenes on heterospin SMM properties[11a] was investigated. In the experimental results, all 1:4 cobalt complexes showed similar SMM properties with a constant U_{eff}/k_B of ca. 90 K, and no dependence of U_{eff}/k_B on the S_{total} value was observed. Furthermore, the τ_Q values were suggested to increase with increasing the S_{total} value. In a series of 1:4 complexes $CoCl_2$(**DXpy**)$_4$, the complex with the smallest S_{total} value of 9/2, $CoCl_2$(**C1py**)$_4$, already had a τ_Q value long enough not to affect the activation barrier, U/k_B.

To reduce the spin multiplicities of the cobalt complexes, this time, bidentate cobalt complex $Co(p\text{-tolsal})_2$, p-tolsal = N-p-tolylsalicylideniminato, was used as the heterospin complex with an S_{total} value smaller than 1:4 complexes, and the magnetic properties before and after irradiation of the 1:2 complexes of $Co(p\text{-tolsal})_2$ and **DXpy** in frozen solution were investigated. The 1:2 complexes $Co(p\text{-tolsal})_2$(**CXpy**)$_2$, **X** = **1**, **2**, **3l**, **3b**, and **4**, were expected to produce the high-spin ground state with S_{total} = 5/2, 9/2, 13/2, 13/2, and 17/2, respectively. The 1:2 complex $Co(p\text{-tolsal})_2$(**cC5py**)$_2$ formed after irradiation of the mixed solution of $Co(p\text{-tolsal})_2$ and cyclic pentadiazopyridine, **cD5py**, has already been reported to function as an SMM with S_{total} = 21/2, U_{eff}/k_B = 72 K, and H_c = 7.1 kOe in frozen solution.[11f]

We report here the relationship between the SMM magnetic properties and the ground-state spin multiplicity in a series of $Co(p\text{-tolsal})_2$(**CXpy**)$_2$, **X** = **1**, **2**, **3l**, **3b**, and **4**, together with $Co(p\text{-tolsal})_2$(**cC5py**)$_2$. In addition, the magnetic properties of $Co(p\text{-tolsal})_2(py)_2$ having no carbene in the absence and presence of a dc field were also reported. In the 1:4 complex $CoCl_2(py)_4$,[11a] the dynamic magnetic behavior showing slow magnetic relaxation with U_{eff}/k_B = 16 K in the presence of a 3 kOe dc field was observed.

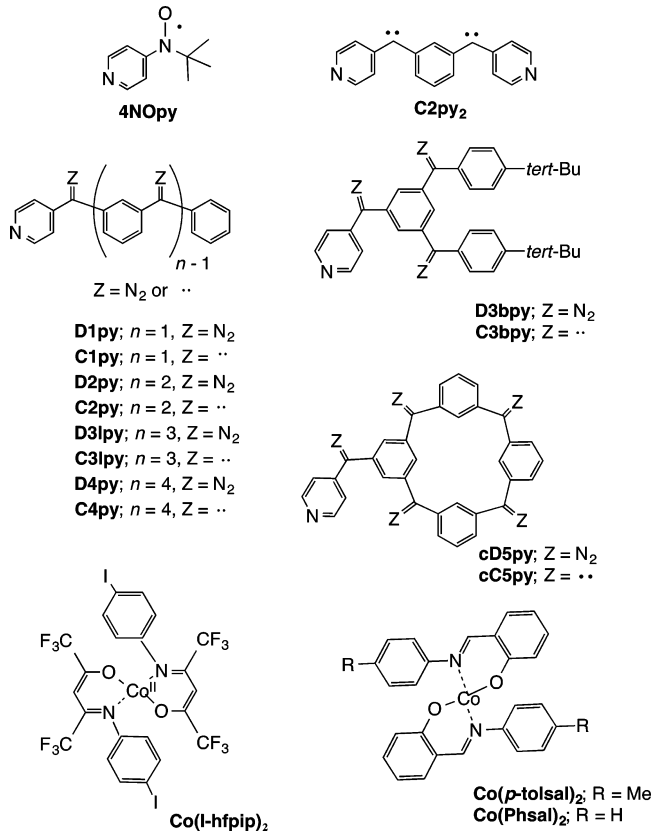

RESULTS AND DISCUSSION

Preparations of DXpy, X = 1, 2, 3l, 3b, and 4, and Their Complexes with Co(p-tolsal)$_2$. Monodiazo-, didiazo-, tridiazo-, and tetradiazopyridine ligands, **DXpy**, **X** = **1**, **2**, **3l**, **3b**, and **4**, were prepared by the procedure reported previously.[11a] **D2py** and **D3bpy** were obtained as single crystals and characterized by X-ray crystallography (S2). The photoproducts after irradiation of **DXpy** were confirmed to be high-spin polycarbene in the ground state by the field dependence of the magnetization in frozen solution.[11a,b] For the preparation of the 1:2 cobalt complexes, solutions of $Co(p\text{-tolsal})_2$ and **DXpy** in degassed CH_2Cl_2 were mixed in a ratio of 1:2 at 4 °C under a nitrogen atmosphere. No single crystals amenable to X-ray structural analysis were obtained with any combination of $Co(p\text{-tolsal})_2$ and **DXpy** at the present stage. The solutions of $Co(p\text{-tolsal})_2$(**DXpy**)$_2$ were relatively unstable in solution, and therefore the solutions were used as samples for the magnetic measurements immediately after mixing $Co(p$-

dx.doi.org/10.1021/ic403074d | Inorg. Chem. 2014, 53, 5447−5457

tolsal)$_2$ and **DXpy** in a ratio of 1:2. In contrast, the 1:2 cobalt complexes [Co(*p*-tolsal)$_2$(py)$_2$] and [Co(Phsal)$_2$(py)$_2$] were obtained as single crystals by mixing the solutions of Co(*p*-tolsal)$_2$ (or Co(Phsal)$_2$) and pyridine.

X-ray Crystallography. Single crystals of [Co(*p*-tolsal)$_2$(py)$_2$] and [Co(Phsal)$_2$(py)$_2$] were analyzed by X-ray crystallography. The complexes were crystallized in space groups $P2_1/c$ and $P\bar{1}$ with $Z = 4$ for [Co(*p*-tolsal)$_2$(py)$_2$] and [Co(Phsal)$_2$(py)$_2$], respectively. In the molecular structures of [Co(*p*-tolsal)$_2$(py)$_2$] and [Co(Phsal)$_2$(py)$_2$], the oxygen atoms of phenoxide in Schiff-base ligands are located at the apical position and two pyridines are coordinated to the cobalt ion in *cis* and *trans* configurations, respectively. Both complexes formed compressed octahedral structures, in which the bond lengths between the cobalt ion and the phenoxide oxygen atoms were shorter by 0.15−0.23 Å than those between the cobalt ion and the imine and pyridine nitrogen atoms. The bond angles of O−Co−O were 179° and 178° for [Co(*p*-tolsal)$_2$(py)$_2$] and [Co(Phsal)$_2$(py)$_2$], respectively. Dihedral angles between the pyridine rings and the *x*−*y* plane defined by the nitrogen atoms of Schiff-base and pyridine ligands were 53−71° and 72−84° for [Co(*p*-tolsal)$_2$(py)$_2$] and [Co(Phsal)$_2$(py)$_2$], respectively. The observed molecular structures were distorted octahedral, similar to those reported previously.[11,12] In the crystal packings, the shortest intermolecular distances between the cobalt ions were 8.38 and 8.80 Å for [Co(*p*-tolsal)$_2$(py)$_2$] and [Co(Phsal)$_2$(py)$_2$], respectively. ORTEP drawings of molecular structures for [Co(*p*-tolsal)$_2$(py)$_2$], [Co(Phsal)$_2$(py)$_2$], **D2py**, and **D3bpy** are shown in Figure S1, and their selected bond lengths, bond angles, and dihedral angles are summarized in Tables S1−S3.

Formation of Co(*p*-tolsal)$_2$(DXpy)$_2$ Complexes in Solution. To confirm the formation of Co(*p*-tolsal)$_2$(**DXpy**)$_2$ in solution, the spectra of vis−NIR and CSI mass for the solution samples were measured.

A. Vis−NIR Spectra of Co(p-tolsal)$_2$(DXpy)$_2$ Complexes. The vis−NIR spectrum of the 1:2 mixture (10 mM) of Co(*p*-tolsal) and **DXpy** in MTHF at room temperature showed a set of weak absorptions at 900 and 1300 nm. On cooling from 288 to 140 K, these absorptions gradually decreased and a new absorption at 950 nm appeared below 190 K. The absorptions at rt and 140 K are characteristic of the d−d transitions of the cobalt(II) ion in the tetrahedral and octahedral coordination structure, respectively,[13,14] indicating that Co(*p*-tolsal)$_2$ and **DXpy** are mostly dissociated at rt but associate to form the 1:2 complex Co(*p*-tolsal)$_2$(**DXpy**)$_2$ at temperatures lower than 140 K. The spectral changes for Co(*p*-tolsal)$_2$(**D3lpy**)$_2$ in the temperature range 288−140 K are shown in Figure S2. The other combination of Co(*p*-tolsal)$_2$ and **DXpy** showed similar spectral changes under similar conditions.

B. Cold-Spray Ionization Mass Spectra. Cold-spray ionization mass spectra[15] for the solution samples were measured at −10 °C using positive mode. The 1:2 mixtures of Co(*p*-tolsal)$_2$ with pyridine and **DXpy** in CH_3CN were used as solution samples. The spectra showed the positive molecular ion peaks with isotope patterns, which were in accordance with the corresponding molecular weight, M^+. The CSI mass spectra for the 1:2 mixtures of Co(*p*-tolsal)$_2$ and **DXpy** are shown in Figure S3 together with the simulation values.

From the results of vis−NIR and CSI mass spectrometry, the complexes formed from the 1:2 mixture of Co(*p*-tolsal)$_2$ and **DXpy** at cryogenic temperature studying the magnetic properties were safely considered to be octahedral, in which **DXpy** coordinated to the cobalt ion as the fifth and the sixth ligand.

Magnetic Properties in Frozen Solution. The solutions (15, 10, 10, 5, and 5 mM, 50 μL) of the 1:2 mixture of Co(*p*-tolsal)$_2$ and **DXpy**, **X** = **1**, **2**, **3l**, **3b**, and **4**, respectively, in MTHF were employed as samples of Co(*p*-tolsal)$_2$(**DXpy**)$_2$ for dc and ac magnetic susceptibility measurements. A solution (50 mM, 50 μL) of [Co(*p*-tolsal)$_2$(py)$_2$] dissolved in MTHF was used as the solution sample.

Photolysis of Co(*p*-tolsal)$_2$(DXpy)$_2$, X = 1, 2, 3l, 3b, and 4, in Frozen Solution. Photolysis of the sample was performed by the procedures reported previously.[11a,b] The *M* vs irradiation time plot for the sample of 1:2 mixture of Co(*p*-tolsal)$_2$(**D3lpy**)$_2$ in MTHF is shown in Figure S4. Quantitative photolysis of the sample was confirmed by the disappearance of the absorption at 2055 cm^{-1} due to the diazo moiety in the IR spectra after SQUID measurements.

A. Static Magnetic Properties in Frozen Solution. A-1. Temperature Dependence of dc Magnetic Susceptibility. The values of dc molar magnetic susceptibility, χ_{mol}, before and after irradiation of Co(*p*-tolsal)$_2$(**DXpy**)$_2$, **X** = **1**, **2**, **3l**, **3b**, and **4**, in frozen solution were collected at a constant field of 5 kOe below 20 K. The obtained χ_{mol} values were plotted as a function of temperature. The plots of $\chi_{mol}T$ vs T before and after irradiation of Co(*p*-tolsal)$_2$(**DXpy**)$_2$, **X** = **1**, **2**, **3l**, **3b**, and **4**, are shown in Figure 1 together with Co(*p*-tolsal)$_2$(py)$_2$.

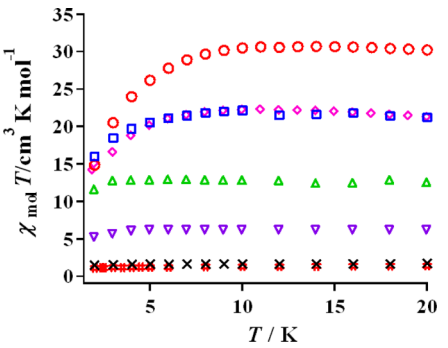

Figure 1. $\chi_{mol}T$ vs T plots of Co(*p*-tolsal)$_2$(**D1py**)$_2$ (black ×), Co(*p*-tolsal)$_2$(**CXpy**)$_2$, X = **1** (purple ▽), **2** (green △), **3l** (blue □), **3b** (pink ◇), and **4** (red circle), and Co(*p*-tolsal)$_2$(py)$_2$ (red #) below 20 K in frozen solution.

The $\chi_{mol}T$ values before irradiation of Co(*p*-tolsal)$_2$(**DXpy**)$_2$ were nearly constant (1.5 cm^3 K mol^{-1}) in the temperature range 1.9−10 K and were close to those for Co(*p*-tolsal)$_2$(py)$_2$. After irradiation, the $\chi_{mol}T$ values for Co(*p*-tolsal)$_2$(**CXpy**)$_2$ were nearly constant depending on the multiplicity of the complexes in the range 5−20 K and gradually decreased below it. The constant $\chi_{mol}T$ values were 6.2, 12.8, 23.8, 24.2, and 32.1 for Co(*p*-tolsal)$_2$(**CXpy**)$_2$, **X** = **1**, **2**, **3l**, **3b**, and **4**, respectively, and were much larger than the theoretical values (3.5, 7.5, 13.5, 13.5, and 21.5 cm^3 $kmol^{-1}$ for Co(*p*-tolsal)$_2$(**CXpy**)$_2$, **X** = **1**, **2**, **3l**, **3b**, and **4**, respectively) calculated by a spin-only equation with two isolated high-spin carbenes (1.0, 3.0, 6.0, 6.0, and 10.0 cm^3 K mol^{-1} × 2) and one high-spin cobalt(II) ion with effective spin $S'_{eff} = 1/2$[16,17] ($\chi_{mol}T$ value of 1.5 cm^3 K mol^{-1} before irradiation). These results suggested that the carbenes and the cobalt ions in the complex interacted ferromagnetically to form a high-spin ground state with S_{total} = 5/2, 9/2, 13/2, 13/2, and 17/2 for Co(*p*-tolsal)$_2$(**CXpy**)$_2$, **X** = **1**, **2**, **3l**, **3b**, and **4**, respectively. The decrease in the $\chi_{mol}T$ values below 10 K

dx.doi.org/10.1021/ic403074d | Inorg. Chem. 2014, 53, 5447−5457

might be due to the effect of the zero-field splitting caused by spin−orbit coupling in the cobalt ion.

A-2. Hysteresis Loops below 3.0 K. The dc magnetization for Co(*p*-tolsal)$_2$(**CXpy**)$_2$, **X** = **1**, **2**, **3l**, **3b**, and **4**, was measured in the range −50 to 50 kOe with a field-sweep rate of 0.35 kOe/s at various temperatures in the range 1.9−3.5 K. The M_{mol} values gradually increased on applying the field and kept on increasing even at 50 kOe, for which the M_{mol} values were 2.0×10^4, 3.8×10^4, 5.2×10^4, 5.6×10^4, and 6.8×10^4 cm^3 Oe mol^{-1} for Co(*p*-tolsal)$_2$(**CXpy**)$_2$, **X** = **1**, **2**, **3l**, **3b**, and **4**, respectively. These values at 50 kOe were lower than those for the values of saturation magnetization, M_s, suggesting that the effect of large spin−orbit coupling operated. In all complexes, hysteresis loops relating to the field appeared below ca. 3.0 K, and the width of the loop increased upon cooling. The hysteresis loops at 1.9 K for Co(*p*-tolsal)$_2$(**CXpy**)$_2$, **X** = **1**, **2**, **3l**, **3b**, and **4**, are summarized in Figure 2, and those at given temperatures together with the H_c vs T plots are shown in Figure S5.

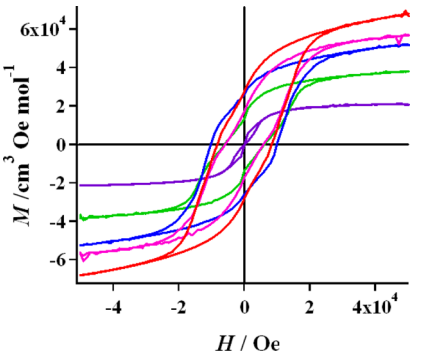

Figure 2. Plots of M_{mol} vs H of Co(*p*-tolsal)$_2$(**CXpy**)$_2$, **X** = **1** (purple), **2** (green), **3l** (blue), **3b** (pink), and **4** (red), at 1.9 K in frozen solution with a sweep rate of 0.35 kOe/s.

In Co(*p*-tolsal)$_2$(**CXpy**)$_2$, **X** = **2**, **3l**, **3b**, and **4**, the coercive force (H_c) and the remnant magnetization (M_r) depended on the temperature. On cooling from 3.0 K, both values gradually increased until 1.9 K. The observed thermal behaviors of H_c and M_r were characteristic of an SMM. The values of H_c and M_r at 1.9 K were ∼0, 6.0, 10, 6.2, and 9.0 kOe and 0, 1.6×10^4, 2.6×10^4, 1.7×10^4, and 2.9×10^4 cm^3 Oe mol^{-1} for Co(*p*-tolsal)$_2$(**CXpy**)$_2$, **X** = **1**, **2**, **3l**, **3b**, and **4**, respectively. The H_c values at 1.9 K increased in the order Co(*p*-tolsal)$_2$(**CXpy**)$_2$, **X** = **1**, **2**, **3b**, **3l**, and **4**, in which those for Co(*p*-tolsal)$_2$(**CXpy**)$_2$, **X** = **3l** and **4**, were close. It was noted that the H_c value for Co(*p*-tolsal)$_2$(**3bpy**)$_2$, having a branched structure, was different from that for the linear isomer, and the value of 6.2 kOe was rather close to that for Co(*p*-tolsal)$_2$(**C2py**)$_2$ and that (7.1 kOe) for Co(*p*-tolsal)$_2$(**cC5py**)$_2$, which had a partial structure of Co(*p*-tolsal)$_2$(**3bpy**)$_2$.

To estimate the D and E values for Co(*p*-tolsal)$_2$(py)$_2$ and Co(*p*-tolsal)$_2$(**C1py**)$_2$, which showed no hysteresis and an extremely weak hysteresis loop at 1.9 K, respectively, the reduced magnetization data in the M_{mol} vs H/T plots were analyzed by using the program ANISOFT 2.0.[18] The best fitting results for Co(*p*-tolsal)$_2$(py)$_2$ and Co(*p*-tolsal)$_2$(**C1py**)$_2$ were −108 and −18 K for D and −0.0008 and −0.0001 K for E values, respectively (Figure S6). The negative D values were obtained, and the large reduction of the $|D|$ value from Co(*p*-tolsal)$_2$(py)$_2$ to Co(*p*-tolsal)$_2$(**C1py**)$_2$ was observed. However, the U/k_B values calculated from $|D|(S^2 - 1/4)$ by using the obtained D values were 216 and 108 K for Co(*p*-tolsal)$_2$(py)$_2$ and Co(*p*-tolsal)$_2$(**C1py**)$_2$, respectively, which were largely different from the following experimental U_{eff}/k_B value. The observed discrepancy was not clear at the present stage.

B. Dynamic Magnetic Properties in Frozen Solution. The dynamic magnetic properties for Co(*p*-tolsal)$_2$(**CXpy**)$_2$, **X** = **1**, **2**, **3l**, **3b**, and **4**, together with a parent complex, Co(*p*-tolsal)$_2$(py)$_2$, were investigated by ac and dc magnetic susceptibility measurements in frozen solution. The ac magnetic susceptibility data were collected with 3.9 or 5.0 Oe ac fields at various frequencies in the temperature range 10−1.9 K. The dc magnetization decays for Co(*p*-tolsal)$_2$(**CXpy**)$_2$, X = **2**, **3l**, **3b**, and **4**, were also measured in the range 3.0−1.9 K.

*B-1. The ac Magnetic Susceptibility Measurements. i. Co(p-tolsal)$_2$(py)$_2$ and Co(p-tolsal)$_2$(**C1py**)$_2$.* The ac magnetic susceptibilities for parent complex Co(*p*-tolsal)$_2$(py)$_2$ were measured with a 3.9 Oe ac field at various frequencies in the temperature range 1.9−10 K. Although both nonzero signals of χ'_{mol} and χ''_{mol} (in-phase and out-of-phase components of ac magnetic susceptibilities, respectively) were observed, no maxima of the signals in the χ'_{mol} and χ''_{mol} vs T plots were observed above 1.9 K (Figure S7-1). By applying the dc field, the maxima of the signals dependent on the frequency appeared in the χ'_{mol} and χ''_{mol} vs T plots. To optimize the applied dc field, the temperature dependencies of χ''_{mol} signals with the frequency of 1.0 Hz were investigated in the presence of dc fields of 1.0, 3.0, and 5.0 kOe. In the χ''_{mol} vs T plots, the dc field of 1.0 kOe showing the maximum intensity of the χ''_{mol} signal was determined as the optimized dc field (Figure S7-2). In the presence of a dc field of 1.0 kOe, the peak-top temperature of χ''_{mol} signals shifted to lower temperature with decreasing frequency (Figure 3a, left) and were below 1.9 K for frequencies lower than 10 Hz. This observation in the absence and presence of a dc field was typical of SMM (or single-ion magnet; SIM) behaviors affected by the QTM pathway. In the absence of a dc field, the QTM relaxation counteracted the slow magnetic relaxation for SMM (SIM), while in the presence of a dc field for suppression of QTM relaxation, the SMM (SIM) behavior was observable. In Co(*p*-tolsal)$_2$(**C1py**)$_2$, in contrast, both χ'_{mol} and χ''_{mol} signals were clearly observed in the absence of a dc field and showed frequency dependence (Figure S8-1 and Figure 3a, right, respectively). As observed in the χ''_{mol} vs T plot, the peak of χ''_{mol} signals had a shoulder below 2.5 K. The χ''_{mol} values at 1.9 K increased with decreasing frequency and eventually were dominant at frequencies less than 1.0 Hz. When the dc field of 1 kOe was applied, the shoulder for the peak of χ''_{mol} signals disappeared (Figure S8-2b), suggesting that the χ''_{mol} signals below 2.5 K might be affected by the relaxation due to the QTM pathway.

The observed thermal profile of the χ''_{mol} signals for Co(*p*-tolsal)$_2$(py)$_2$ and Co(*p*-tolsal)$_2$(**C1py**)$_2$ might suggest that the magnetic relaxations through thermodynamic and QTM pathways were observed at high and low temperatures, respectively. To estimate the relaxation time at low temperature, the χ''_{mol} values in the χ''_{mol} vs T plot were analyzed by the Debye model[19] and were plotted as a function of frequency (Figure 3b). The τ values obtained from the plots of χ''_{mol} vs T and χ''_{mol} vs frequency were combined and plotted as a function of inverse T (Figure 3c). In the τ vs T^{-1} plots, on cooling, the τ values almost linearly increased in the high-temperature region and deviated from the straight line at low temperature. The relaxation in the high-temperature region obeyed the Arrhenius

dx.doi.org/10.1021/ic403074d | Inorg. Chem. 2014, 53, 5447−5457

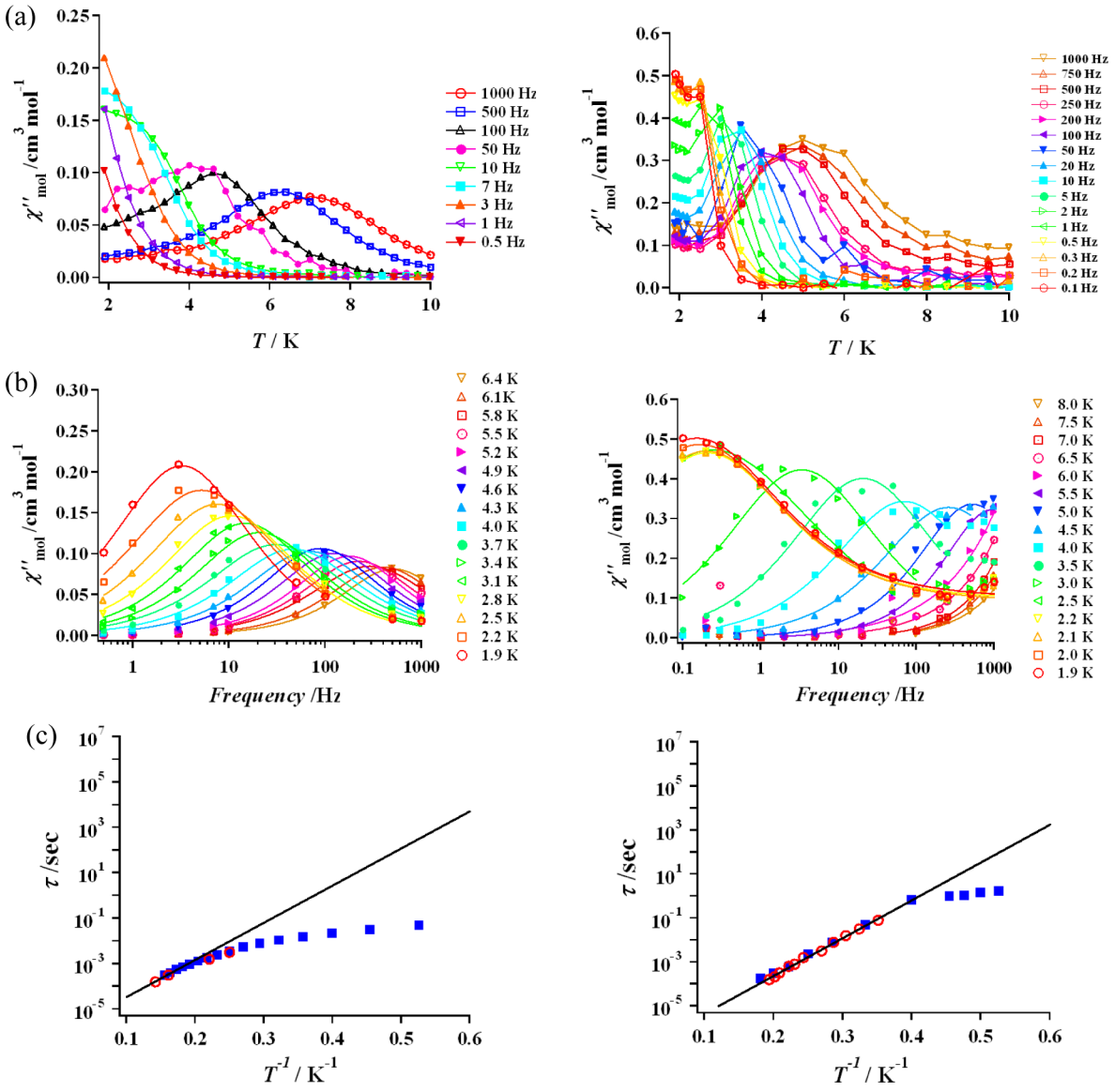

Figure 3. Plots of (a) χ''_{mol} vs T, (b) χ''_{mol} vs frequency, and (c) τ vs T^{-1} for Co(p-tolsal)$_2$(py)$_2$ (left) and Co(p-tolsal)$_2$(**C1py**)$_2$ (right) in the presence and absence of a dc field of 1 kOe, respectively. The solid lines in (a) and (b) are visual guides and fitted curves by the Debye model, respectively. In (c), the red circles and blue squares are τ values obtained from the plots of χ''_{mol} vs T and χ''_{mol} vs frequency, respectively, and the straight lines are obtained by the Arrhenius law using the data at 1000, 750, 500, 250, and 200 Hz in the χ''_{mol} vs T plot.

law; $\tau = 1/(2\pi\nu) = \tau_0 \exp(U_{eff}/k_BT)$. From the straight line in the τ vs T^{-1} plots, the effective activation energy, U_{eff}/k_B, and the pre-exponential factor, τ_0, were estimated. In Co(p-tolsal)$_2$(py)$_2$, the values of U_{eff}/k_B and τ_0 in the presence of 1.0 kOe were estimated to be 38 K and 8.0 × 10^{-7} s, respectively. The τ values obtained by the Debye model deviated downward from the straight line below 4.0 K and reached a near-plateau (0.05 s) at 1.9 K. In the absence of a dc field, on the other hand, values of U_{eff}/k_B of 40 K and τ_0 of 8.0 × 10^{-8} s were obtained for Co(p-tolsal)$_2$(**C1py**)$_2$. The τ values below 2.5 K obtained from the χ''_{mol} vs frequency plot deviated from the straight line for the Arrhenius plot and approached a constant value. The relaxation time, $\tau_{1.9}$, of 1.6 s at 1.9 K might be close to the relaxation time, τ_Q, due to QTM, which was temperature independent. Applying a dc field of 1 kOe, the deviation below 2.5 K in the τ vs T^{-1} plot disappeared and values of U_{eff}/k_B of 42 K and τ_0 of 5.2 × 10^{-8} s were obtained (Figure S8-2d). The values obtained in the absence and presence of a dc field were ca. 40 K and similar to each other. This result indicated that the contribution of QTM relaxation to the U_{eff}/k_B value for Co(p-tolsal)$_2$(**C1py**)$_2$ was insignificant and the relaxation below 2.5 K was controlled by QTM.

The χ''_{mol} vs T, χ''_{mol} vs frequency, and Arrhenius plots for Co(p-tolsal)$_2$(py)$_2$ and Co(p-tolsal)$_2$(**C1py**)$_2$ in the presence and absence of a dc field (1 kOe), respectively, are shown in Figure 3, and those for Co(p-tolsal)$_2$(**C1py**)$_2$ in the presence of a dc field (1 kOe) are shown in Figure S8-2.

The microcrystalline samples of [Co(p-tolsal)$_2$(py)$_2$] and [Co(Phsal)$_2$(py)$_2$], which had a *cis* and *trans* configuration, respectively, also showed similar magnetic behavior in the absence and presence of a dc of 1.0 kOe, which are shown in Figure S9-1 and S9-2 for [Co(p-tolsal)$_2$(py)$_2$] and in Figure S9-3 and S9-4 for [Co(Phsal)$_2$(py)$_2$]. The values of U_{eff}/k_B and τ_0 of 35 and 34 K and 1.2 × 10^{-6} and 3.3 × 10^{-7} s for [Co(p-tolsal)$_2$(py)$_2$] and [Co(Phsal)$_2$(py)$_2$], respectively, in the presence of a dc of 1.0 kOe were obtained. These results

dx.doi.org/10.1021/ic403074d | *Inorg. Chem.* 2014, 53, 5447−5457

suggest that the coordination geometry of pyridine in these cobalt complexes did not largely affect the U_{eff}/k_B values.

The parent complex Co(*p*-tolsal)$_2$(py)$_2$ is a high-spin cobalt(II) complex with noninteger spin. In the easy-axis (D < 0) noninteger spin system, the transverse anisotropy should not affect the QTM pathway according to Kramers' theorem. In addition, the measuring conditions, which were the presence of a dc field and in frozen solution, might eliminate the contribution of the dipole interaction and the hyperfine coupling to QTM. However, the observed magnetic behaviors in the absence and presence of a dc field suggested that Co(*p*-tolsal)$_2$(py)$_2$ had a non-negligible QTM pathway within a molecule. Recently, similar results for complexes containing high-spin cobalt(II) ions have been reported.[6] In contrast, Co(*p*-tolsal)$_2$(**C1py**)$_2$ showed a slow magnetic relaxation with the U_{eff}/k_B value in the absence of dc field, indicating that the generating carbene magnetically coupled with the cobalt ion to suppress the relaxation through the QTM pathway.

*ii. Co(p-tolsal)$_2$(**CXpy**)$_2$, **X** = **2**, **3l**, **3b**, and **4**.* The ac magnetic susceptibilities of Co(*p*-tolsal)$_2$(**CXpy**)$_2$, **X** = **2**, **3l**, **3b**, and **4**, were measured under conditions similar to those for Co(*p*-tolsal)$_2$(**C1py**)$_2$. Both χ'_{mol} and χ''_{mol} signals depending on the frequency were clearly observed in the absence of a dc field. The $\chi'_{mol}T$ vs T plots are shown in Figure S10. The χ''_{mol} vs T plots are shown in Figure 4 for Co(*p*-tolsal)$_2$(**CXpy**)$_2$, **X** = **2**, **3l**, and **4**, and Figure S11 for Co(*p*-tolsal)$_2$(**C3bpy**)$_2$.

In the plot of $\chi'_{mol}T$ vs T, the values of $\chi'_{mol}T$ were 13.5, 23.7, 22.7, and 33.3 cm^3 K mol^{-1} at 10 K for Co(*p*-tolsal)$_2$(**CXpy**)$_2$, **X** = **2**, **3l**, **3b**, and **4**, respectively, and remained essentially constant on cooling to ~5 K. Below 5 K, the $\chi'_{mol}T$ values with frequency dependence decreased, while the χ''_{mol} signals appeared at the same temperature. In the χ''_{mol} vs T plot, the χ''_{mol} signals with frequency dependence were also observed above 1.9 K, and the maximum χ''_{mol} signals shifted to lower temperature with decreasing frequency. From each frequency ($1/4\pi\tau$) at the peak-top temperature for χ''_{mol}, the values for U_{eff}/k_B and τ_0 were obtained in terms of the Arrhenius equation. The values of U_{eff}/k_B and τ_0 for Co(*p*-tolsal)$_2$(**CXpy**)$_2$, **X** = **2**, **3l**, **3b**, and **4**, were estimated to be 65, 73, 72, and 74 K, and 4.4×10^{-9}, 1.5×10^{-9}, 1.1×10^{-9}, and 1.6×10^{-9} s, respectively (Figure 7). The U_{eff}/k_B and τ_0 values of the isomeric complexes Co(*p*-tolsal)$_2$(**C3bpy**)$_2$ and Co(*p*-tolsal)$_2$(**C3lpy**)$_2$ were close to each other, indicating that the structural difference did not affect the U_{eff}/k_B value. Those for Co(*p*-tolsal)$_2$(**cC5Py**)$_2$ were reported[11f] to be 72 K and 2.0×10^{-9} s, respectively. The obtained τ_0 values, which were smaller than those of typical SMMs,[2] were close to those of SMMs with large S_{total} values reported previously.[2c,d,20]

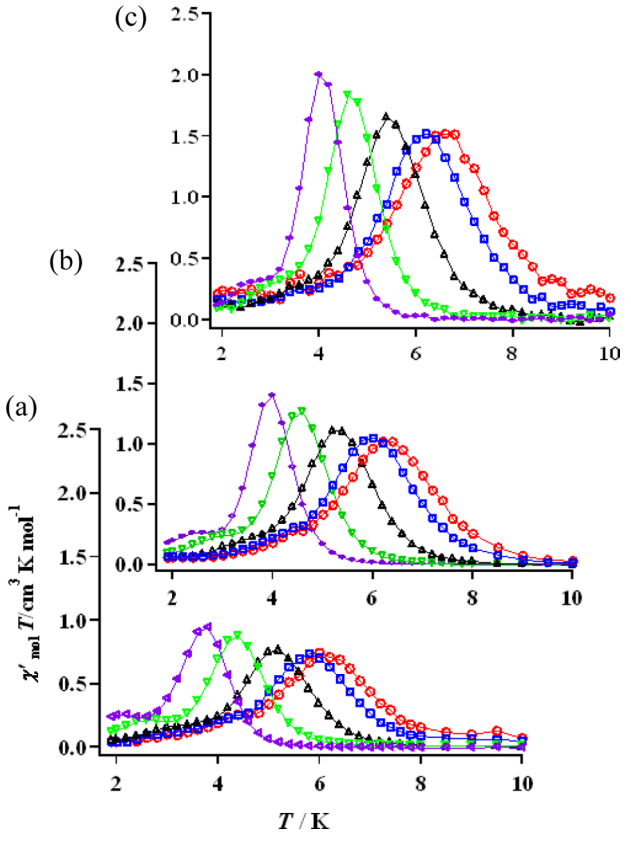

Figure 4. Plots of χ''_{mol} vs T of Co(*p*-tolsal)$_2$(**CXpy**)$_2$, **X** = (a) **2**, (b) **3l**, and (c) **4**, in frozen MTHF solution with a 5 Oe ac field oscillating at 1 (◇), 10 (▼), 100 (▲), 500 (■), and 1000 (●) Hz. The solid lines are visual guides.

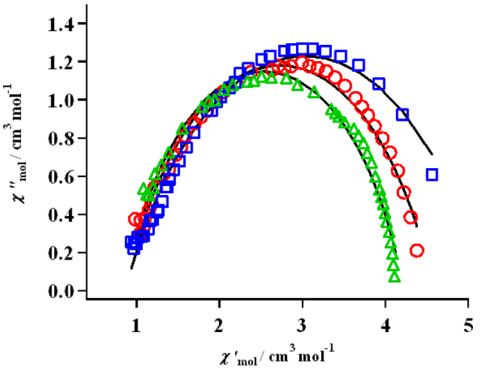

Figure 5. Plot of χ'_{mol} vs χ''_{mol} at 4.5 (blue □), 4.9 (red ○), and 5.3 (green △) K for Co(*p*-tolsal)$_2$(**C3lpy**)$_2$. Solid lines are a least-squares fitting of the data to the distribution of a single relaxation process.

In order to investigate the relaxation process due to the cobalt complexes in frozen solutions in more detail, further ac magnetic susceptibility measurements were carried out. The ac magnetic susceptibility data after irradiation of the 1:2 mixture, Co(*p*-tolsal)$_2$(**D3lpy**)$_2$, in frozen MTHF solution were collected by holding at various constant temperatures and varying the frequency of the ac field (5 Oe) from 1000 to 1 Hz. The plots of χ'_{mol} vs frequency and χ''_{mol} vs frequency at 4.5, 4.9, and 5.3 K are shown in Figure S12, and that of χ'_{mol} vs χ''_{mol} (Cole−Cole diagram) is shown in Figure 5.

The frequency dependences of χ'_{mol} and χ''_{mol} at constant temperatures were analyzed by a Debye model, and the fitted curves are shown as solid lines in Figure S12. The Cole−Cole plot[21] shown in Figure 5, which is nearly symmetric with distribution widths α = 0.23, 0.28, and 0.34 at 5.3, 4.9, and 4.5 K, respectively, indicated that a single relaxation process was present in the Co(*p*-tolsal)$_2$(**C3lpy**)$_2$. The obtained α values were relatively large, which suggested that there was a distribution in the single relaxation process. This distribution would be mainly due to the frozen solution condition used for the formation of SMM.

*B-2. The dc Magnetization Decay for Co(p-tolsal)$_2$(**CXpy**)$_2$, **X** = **2**, **3l**, **3b**, **4**, and Co(p-tolsal)$_2$(**cC5py**)$_2$.* To characterize the slow magnetization relaxation at even lower temperatures, the dc magnetization decay experiments for Co(*p*-tol-

dx.doi.org/10.1021/ic403074d | Inorg. Chem. 2014, 53, 5447−5457

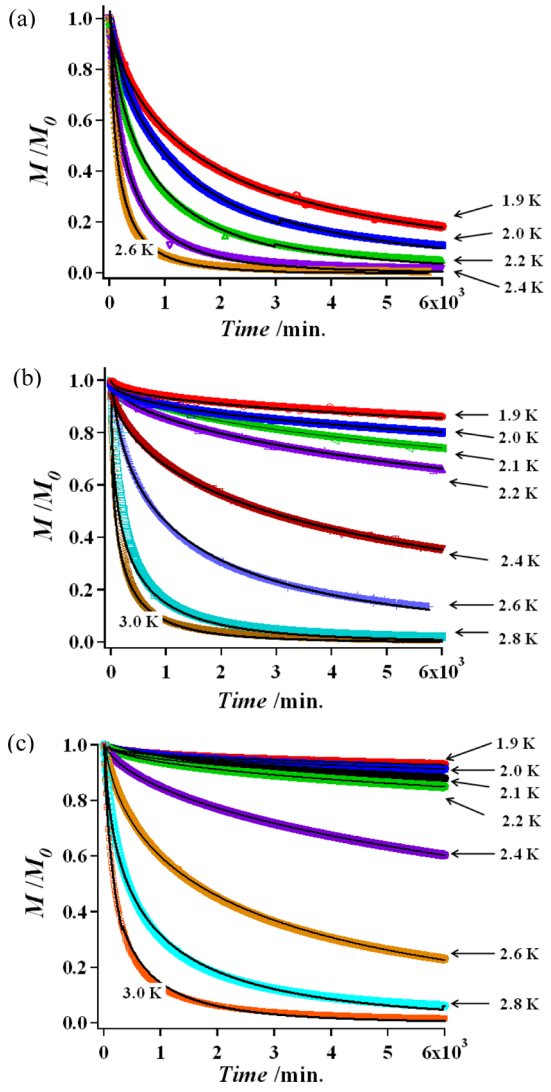

Figure 6. The dc magnetization decays for (a) Co(*p*-tolsal)$_2$(**C2py**)$_2$, (b) Co(*p*-tolsal)$_2$(**C3lpy**)$_2$, and (c) Co(*p*-tolsal)$_2$(**C4py**)$_2$, at given temperatures, after applying a field of 50 and reducing to 0 kOe. Solid lines show the fitting results by the stretched exponential equation.

sal)$_2$(**CXpy**)$_2$, **X** = **2**, **3l**, **3b**, and **4**, were carried out in the temperature range 1.9−3.0 K. In addition, the decay experiment for Co(*p*-tolsal)$_2$(**cC5py**)$_2$, which had the largest S_{car} value of 10/2, was also carried out under a similar condition. After the cycle of applying the field of 50 kOe at 10 K, cooling to the desired temperature, and then reducing to 0 kOe, the magnetizations were measured as a function of time. The measurements were performed at various temperatures in the range 2.8−1.9 K. For each measurement, the temperature was raised to 10 K once and then cooled to the desired temperature. The magnetization data, M, were normalized by that, M_0, at t = 0 at each temperature and were plotted as M/M_0 vs time. The decay curves at each given temperature are shown in Figure 6 for Co(*p*-tolsal)$_2$(**CXpy**)$_2$, **X** = **2**, **3l**, and **4**, and in Figure S13 for Co(*p*-tolsal)$_2$(**C3bpy**)$_2$ and Co(*p*-tolsal)$_2$(**cC5py**)$_2$.

The dc magnetization decays for Co(*p*-tolsal)$_2$(**CXpy**)$_2$, **X** = **2**, **3l**, **3b**, and **4**, and Co(*p*-tolsal)$_2$(**cC5py**)$_2$ became slower on cooling, and their decay times at the same temperature decreased in the order Co(*p*-tolsal)$_2$(**CXpy**)$_2$, **X** = **2**, **3**, and **4**, and Co(*p*-tolsal)$_2$(**cC5py**)$_2$. However, the decay times above 1.9 K did not reach constant values, determining that the decay times were due to QTM. To obtain the relaxation times for Co(*p*-tolsal)$_2$(**CXpy**)$_2$, **X** = **2**, **3l**, **3b**, and **4**, and Co(*p*-tolsal)$_2$(**cC5py**)$_2$, the experimental decay data were fitted to a stretched exponential decay (eq 1).[11a,b,22]

$$\ln(M) = \ln(M_0) - (t/\tau)^B \quad (1)$$

where M_0 is the initial magnetization, τ is the average relaxation time, and B is the width of the distribution; B = 1 is a single-exponential decay. Taking the magnitude of the M_0 value ($M_0(T)$; M_0 at T, > $0.5M_0(1.9)$) into account, in which the values of $M_0(1.9)$ for Co(*p*-tolsal)$_2$(**CXpy**)$_2$, **X** = **2**, **3l**, **3b**, and **4**, and Co(*p*-tolsal)$_2$(**cC5py**)$_2$ were 31, 46, 31, 47, and 35%, respectively, of the M value at 50 kOe, the experimental decay data were selected and the data in the temperature ranges 1.9−2.2, 1.9−2.6, 1.9−2.6, 2.0−2.6, and 2.1−2.8 K for Co(*p*-tolsal)$_2$(**CXpy**)$_2$, **X** = **2**, **3l**, **3b**, and **4**, and Co(*p*-tolsal)$_2$(**cC5py**)$_2$ were used for the fitting experiments. The τ values in the range 10^3−10^5 s with B values in the range 0.4−0.6 were obtained. The values of τ and B obtained by a stretched exponential decay are listed in Table 1 together with the relaxation times for Co(*p*-tolsal)$_2$(**C1py**)$_2$ obtained by the Debye model, and the fitting curves are shown in Figure 6 as solid lines.

Magnetic Relaxations in Co(*p*-tolsal)$_2$(CXpy)$_2$, X = 2, 3l, 3b, and 4. In SMM, the characteristic slow magnetic relaxation for the reorientation of the magnetization takes place in two pathways due to U/k_B and QTM. The relaxations due to the former are temperature-dependent and obtained by the ac magnetic susceptibility technique, while those for the latter are temperature-independent and determined by the temperature dependence of the dc magnetization decay at extremely low temperature. For Co(*p*-tolsal)$_2$(**CXpy**)$_2$, **X** = **2**, **3l**, and **4**, and Co(*p*-tolsal)$_2$(**cC5py**)$_2$, the dc magnetization decays are combined with those given by means of the ac magnetic susceptibility technique and are shown as τ vs T^{-1} plots in Figure 7. The τ vs T^{-1} plot for Co(*p*-tolsal)$_2$(**C3bpy**)$_2$ is shown in Figure S14.

In the higher temperature region, the decay obeyed the Arrhenius law, while in the lower temperature region, the τ values for Co(*p*-tolsal)(**CXpy**)$_2$ collected by the dc magnetization decay deviated downward from the extrapolation of the linear Arrhenius plot obtained by the ac magnetic susceptibility technique. The observed deviation suggests that the τ values in the low-temperature region (<3.0 K) were affected by the τ_Q. In addition, the degree of deviation became smaller in the order Co(*p*-tolsal)$_2$(**CXpy**)$_2$, **X** = **2**, **3l**, **3b**, and **4**, suggesting that the contribution of τ_Q due to RQT relaxation became smaller with increasing S_{total} value. Accordingly, the τ_Q values might become larger with increasing S_{total} value. Actually, the τ values at a given temperature below 3 K for Co(*p*-tolsal)$_2$(**cC5py**)$_2$, which had the largest S_{total} value, were traced on a straight line, and no deviation was observed until 1.9 K. Although the τ_Q values for Co(*p*-tolsal)$_2$(**CXpy**)$_2$, **X** = **2**, **3l**, **3b**, and **4**, could not be determined, they were estimated to be ∼2 × 10^3 s for Co(*p*-tolsal)$_2$(**C2py**)$_2$ and >10^5 s for Co(*p*-tolsal)$_2$(**CXpy**)$_2$, **X** = **3l**, **3b**, and **4**, from the τ values at 1.9 or 2.0 K.

Role of Carbene in SMM Behaviors of 1:2 Complexes of Co(*p*-tolsal)$_2$(CXpy)$_2$ in Frozen Solution. The 1:2 cobalt complexes with S_{total} = 3/2−21/2 showed heterospin SMM behaviors, and their thermal activation barriers partially depended on the S_{total} values due to carbene multiplicity. All magnetic physical values for Co(*p*-tolsal)$_2$(py)$_2$ and Co(*p*-

dx.doi.org/10.1021/ic403074d | Inorg. Chem. 2014, 53, 5447−5457

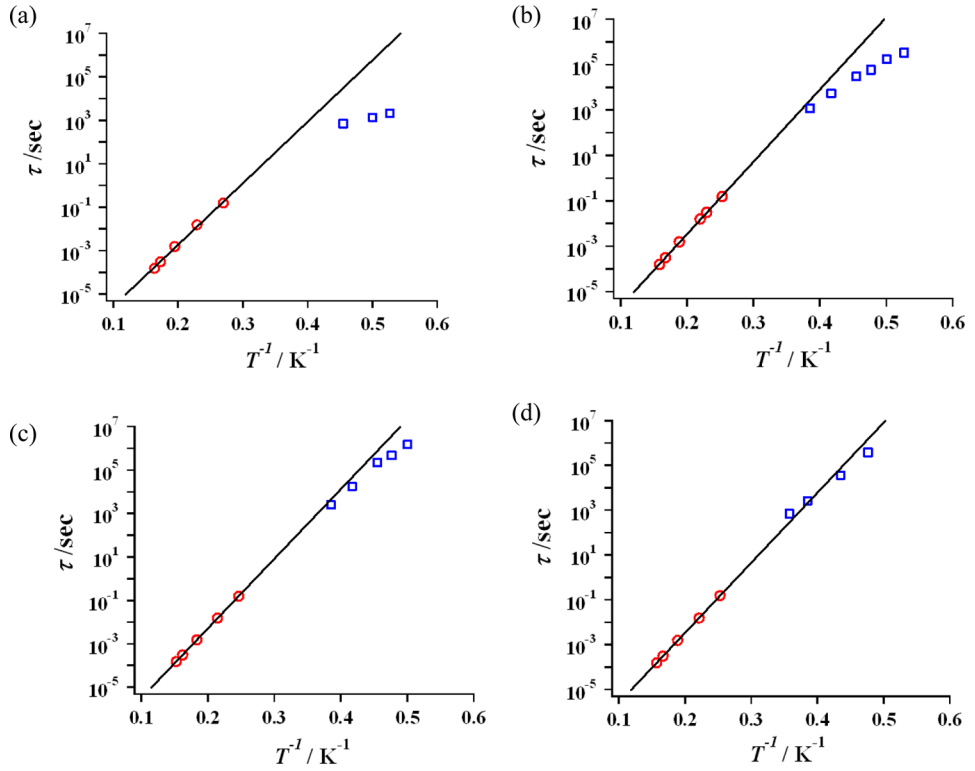

Figure 7. Plots of τ vs T^{-1} for Co(p-tolsal)$_2$(**CXpy**)$_2$, **X** = (a) **2**, (b) **3l**, (c) **4**, and (d) Co(p-tolsal)$_2$(**cC5py**)$_2$. The symbols of red circles and blue squares indicate the τ data collected by ac magnetic susceptibility technique and by dc magnetization decay, respectively. The solid lines are the least-squares fits of the ac data (red circles) according to the Arrhenius equation.

Table 1. Values of Average Relaxation Time, τ, and Distribution Parameter, B, in Parentheses for Co(p-tolsal)$_2$(CXpy)$_2$, X = 2, 3l, 3b, and 4, and Co(p-tolsal)$_2$(cC5py)$_2$, Together with Those for Co(p-tolsal)$_2$(C1py)$_2$ at Various Temperatures below 2.8 K

	τ/s					
T/K	Co(p-tolsal)$_2$(**C1py**)$_2$	Co(p-tolsal)$_2$(**C2py**)$_2$	Co(p-tolsal)$_2$(**C3lpy**)$_2$	Co(p-tolsal)$_2$(**C3bpy**)$_2$	Co(p-tolsal)$_2$(**C4py**)$_2$	Co(p-tolsal)$_2$(**cC5py**)$_2$
1.9	1.6[a]	2.2×10^3 (0.62)	3.6×10^5 (0.44)	2.8×10^5 (0.50)	n.e.[b]	n.e.
2.0	1.4[a]	1.4×10^3 (0.66)	1.8×10^5 (0.45)		2.5×10^5 (0.42)	n.e.
2.1	1.0[a]		5.1×10^4 (0.57)	6.0×10^4 (0.53)	7.7×10^4 (0.45)	3.9×10^5 (0.51)
2.2		7.3×10^2 (0.61)	2.8×10^4 (0.58)	2.0×10^4 (0.57)	3.7×10^4 (0.48)	
2.3						3.8×10^4 (0.60)
2.4		n.e.	2.3×10^3 (0.54)	3.6×10^3 (0.54)	2.9×10^4 (0.59)	
2.6		n.e.	1.2×10^3 (0.51)	8.2×10^2 (0.50)	4.2×10^3 (0.54)	2.7×10^3 (0.62)
2.8			n.e.	n.e.	n.e.	7.2×10^2 (0.54)

[a]Value obtained by a least-squares method using the data for the Debye plot. [b]n.e., not estimated.

tolsal)$_2$(**CXpy**)$_2$, **X** = **1**, **2**, **3l**, **3b**, and **4**, are summarized in Table 2 together with those for Co(p-tolsal)$_2$(**cC5py**)$_2$.

The U_{eff}/k_B value in SMM is mainly determined by the relative ratio for the thermodynamic and the QTM relaxation times (τ and τ_Q, respectively) in both pathways, which are temperature dependent and independent, respectively. Co(p-tolsal)$_2$(py)$_2$, having no carbene, showed no SMM behavior in the absence of a dc field, suggesting that the τ_Q was faster than τ and counteracted the SMM behavior. Applying the dc field (1 kOe) for depression of the QTM pathway elicited an SMM behavior with a U_{eff}/k_B of 38 K. In contrast, in the absence of a dc field, Co(p-tolsal)$_2$(**C1py**)$_2$ exhibited an SMM behavior with a U_{eff}/k_B of 40 K, whose value was close to that for Co(p-tolsal)$_2$(py)$_2$ in the presence of a dc field. This result suggested that carbene magnetically interacted with the cobalt ion to suppress the QTM pathway and make the τ_Q value large. Actually, in Co(p-tolsal)$_2$(**CXpy**)$_2$, **X** = **1**, **2**, **3l**, **3b**, and **4**, the τ_Q values depended on the S_{total} value. The τ_Q value for Co(p-tolsal)$_2$(**C1py**)$_2$ with S_{total} = 5/2 was 1.6 s, which was sufficiently longer than τ used to determine the activation barrier (Figure 3c, right). Furthermore, the τ_Q value for Co(p-tolsal)$_2$(**C2py**)$_2$ with S_{total} = 9/2 was ca. 2×10^3 s and much longer than the time scale for ac measurements. In Co(p-tolsal)$_2$(**CXpy**)$_2$, **X** = **3** and **4**, and Co(p-tolsal)$_2$(**cC5py**)$_2$ with S_{total} = 13/2, 17/2, and 21/2, respectively, although accurate values of τ_Q for **3**, **4**, and Co(p-tolsal)$_2$(**cC5py**)$_2$ could not be determined and were extremely slow (>10^5 s), a tendency for the τ_Q values to increase with increasing S_{total} value was observed; the deviation of the data obtained from the dc decay became small in the order **3**, **4**, and Co(p-tolsal)$_2$(**cC5py**)$_2$ (Figure 6). In Co(p-tolsal)$_2$(**CXpy**)$_2$, **X** = **1**, **2**, **3l**, **3b**, and **4**, and Co(p-tolsal)$_2$(**cC5py**)$_2$, therefore, the τ_Q increased with increasing S_{total} and the contribution of QTM relaxation to the obtained U_{eff}/k_B value could be eliminated.

dx.doi.org/10.1021/ic403074d | Inorg. Chem. 2014, 53, 5447−5457

Table 2. Magnetic Physical Data for Co(*p*-tolsal)$_2$(py)$_2$, Co(*p*-tolsal)$_2$(CXpy)$_2$, X = 1, 2, 3l, 3b, and 4, and Co(*p*-tolsal)$_2$(cC5py)$_2$ in Frozen Solution

1:2 complexes	S_{total}	U_{eff}/K	τ_0/s	τ_Q/s	H_c[a]/kOe
Co(*p*-tolsal)$_2$(py)$_2$[b]	3/2	38[b,c]	8.0×10^{-7}	~0.05[b,c]	0
Co(*p*-tolsal)$_2$(**C1py**)$_2$	5/2[d]	40	8.4×10^{-8}	1.6[c]	~ 0
Co(*p*-tolsal)$_2$(**C2py**)$_2$	9/2[d]	65	4.4×10^{-9}	$\sim 2 \times 10^3$	6.2
Co(*p*-tolsal)$_2$(**C3lpy**)$_2$	13/2[d]	73	1.5×10^{-9}	$>10^5$	10
Co(*p*-tolsal)$_2$(**C3bpy**)$_2$	13/2[d]	72	1.1×10^{-9}	$>10^5$	6.0
Co(*p*-tolsal)$_2$(**C4py**)$_2$	17/2[d]	74	1.6×10^{-9}	$>10^5$	9.0
Co(*p*-tolsal)$_2$(**cC5py**)$_2$[e]	21/2[d]	72	2.0×10^{-9}	$>10^5$	7.1

[a]At 1.9 K. [b]In the presence of a 1.0 kOe dc field. [c]τ value at 1.9 K obtained by the Debye model. [d]Calculated as effective spin ($S' = 1/2$) for the cobalt ion. [e]Ref 11f.

In contrast, the dependence of U_{eff}/k_B on S_{total} showed a profile different from the relationship between τ_Q and S_{total}. The U_{eff}/k_B vs S_{total} plot is shown in Figure 8.

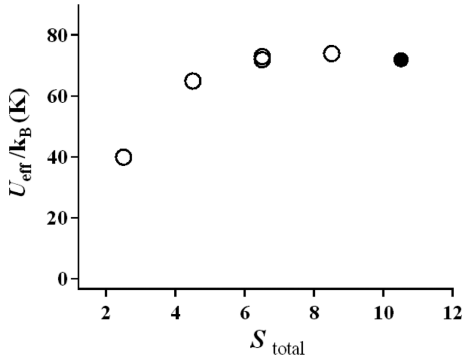

Figure 8. Plot of U_{eff}/k_B vs S_{total} for Co(*p*-tolsal)$_2$(**CXpy**)$_2$, **X** = **1**, **2**, **3l**, **3b**, **4** (open circles), and Co(*p*-tolsal)$_2$(**cC5py**)$_2$ (filled circles).

The dependence of U_{eff}/k_B on S_{total} for Co(*p*-tolsal)$_2$(**CXpy**)$_2$ and Co(*p*-tolsal)$_2$(**cC5py**)$_2$ had a critical S_{total} value, S_c, of 13/2 and showed a different dependence below and above S_c, as shown in Figure 8. Below S_c, the U_{eff}/k_B values increased in the order 40, 65, and 74 K at S_{total} values of 5/2, 9/2, and 13/2, respectively, while above S_c values of 13/2, the U_{eff}/k_B values were constant (ca. 70 K). Since in these 1:2 cobalt−carbene complexes the contribution of QTM relaxation to the thermodynamic activation barrier, U/k_B, for the orientation of magnetic moments could be ignored, the U_{eff}/k_B ($\sim U/k_B$) values could be considered as the equation $|D|(S^2 - 1/4)$ for noninteger spin. Therefore, the U_{eff}/k_B values for Co(*p*-tolsal)$_2$(**CXpy**)$_2$, **X** = **1**, **2**, **3l**, **3b**, and **4**, and Co(*p*-tolsal)$_2$(**cC5py**)$_2$ corresponded to 6|*D*|, 20|*D*|, 42|*D*|, 42|*D*|, 72|*D*|, and 110|*D*|, respectively, and the |*D*| values were estimated to be 6.6, 3.2, 1.5, 1.5, 1.0, and 0.65 K, respectively, indicating that the |*D*| values decreased with increasing the S_{total} value in Co(*p*-tolsal)$_2$(**CXpy**)$_2$ and Co(*p*-tolsal)$_2$(**cC5py**)$_2$. Relating to the |*D*| value,[23] the magnetic couplings between the cobalt ion and the carbene ($|D|/hc$ = 0.434 and $|E|/hc$ = 0.020 cm^{-1} for **C1py**)[24] would reduce the |*D*| value. Therefore, the |*D*| values would be smaller in the order Co(*p*-tolsal)$_2$(**py**)$_2$ and Co(*p*-tolsal)$_2$(**CXpy**)$_2$, **X** = **1**, **2**, **3l**, **3b**, and **4**, and Co(*p*-tolsal)$_2$(**cC5py**)$_2$. This order was consistent with that of the |*D*| values calculated from $|D|(S^2 - 1/4)$. Below S_c, the increase of U_{eff}/k_B for Co(*p*-tolsal)$_2$(**CXpy**)$_2$, **X** = **1**, **2**, and **3**, might be due to the increase of S_{total} accompanied by the decrease of |*D*|. In contrast, above S_c, the constant values of ca. 70 K for U_{eff}/k_B of Co(*p*-tolsal)$_2$(**CXpy**)$_2$, **X** = **3l**, **3b**, and **4**, and Co(*p*-tolsal)$_2$(**cC5py**)$_2$ could be explained in a similar way; the constant U_{eff}/k_B value of ca. 70 K could be obtained by the increase of S_{total} with a decrease of |*D*| using the equation $U/k_B = |D|(S^2 - 1/4)$. However, in the large spin system with relatively small exchange coupling,[25] generally, the contribution of the low-lying thermally excited state to the ground state might be large and increase with increasing S_{total} value. In Co(*p*-tolsal)$_2$(**CXpy**)$_2$, **X** = **3l**, **3b**, **4**, and Co(*p*-tolsal)$_2$(**cC5py**)$_2$, being above S_c, the observed spin multiplicities in the ground state did not correspond to the S_{total} value. The large participations of the low-lying thermally excited state in the ground state might lead the U_{eff}/k_B values of the complexes over S_{total} = 13/2 to become constant (ca. 70 K). In the polymetal cluster systems with high-spin ground states, actually, similar participations in the ground state have been reported.[2c,d,20] Similar results were also observed in the 1:4 Co−carbene complexes.[11a,b] In the experiments using Co(Cl$_2$)(**CXpy**)$_4$, **X** = **1**, **2**, **3l**, **3b**, and **4**, with S_{total} = 9/2−33/2, the obtained U_{eff}/k_B values for all complexes were nearly constant at 90 K. This result suggested the possibility that the U_{eff}/k_B value did not depend on the multiplicity, S_{car}, of carbenes in heterospin SMM. In this study using the 1:2 complexes, however, the result that, when the S_{total} value was smaller than S_c = 13/2, the U_{eff}/k_B value depended on S_{total} and increased with increasing S_{total} value, eliminated such a possibility. The S_{total} value of 9/2 for Co(Cl)$_2$(**C1py**)$_4$, which was the smallest value in Co(Cl)$_2$(**CXpy**)$_4$, might already be above the value of S_c for the 1:4 complexes.

CONCLUSION

A parent complex Co(*p*-tolsal)$_2$(py)$_2$ showed no SMM behavior in the absence of a dc field and showed an SMM behavior in the presence of a dc field. This result could be explained by the SMM behavior for Co(*p*-tolsal)$_2$(py)$_2$ being counteracted by the fast relaxations through the QTM pathway and the QTM relaxation being suppressed by applying a static dc field. In contrast, the 1:2 complexes Co(*p*-tolsal)$_2$(**DXpy**)$_2$, **X** = **1**, **2**, **3**, and **4**, showed SMM behaviors after irradiation. This result suggested that the magnetic coupling between carbene and the cobalt ion suppressed the QTM pathway, leading to SMM behavior being observable. In the generated high-spin cobalt−carbene complexes with S_{total} = 5/2, 9/2, 13/2, and 17/2 after irradiation, the QTM relaxation time, τ_Q, depended on the S_{total} of the complex, and the τ_Q value increased with increasing S_{total} value. On the other hand, the obtained effective activation barrier, U_{eff}/k_B, also depended on the S_{total} value, which had a critical value, S_c. Below S_c, the U_{eff}/k_B value increased with increasing S_{total} value according to the equation $U_{eff}/k_B = |D|(S^2 - 1/4)$, in which |*D*| decreased with increasing S_{total}. Above S_c, the high-spin ground state was affected by the large contribution of the low-lying excited state to provide heterospin SMM complexes with constant U_{eff}/k_B values.

In conclusion, the organic spin in a heterospin complex was considered to be a useful tool for suppressing the QTM pathway for the construction of an SMM with a relatively large

dx.doi.org/10.1021/ic403074d | Inorg. Chem. 2014, 53, 5447−5457

activation barrier for reorientation of the magnetic moment. The observed heterospin SMM properties might be due to the location of the organic spin in the cobalt complex. In Co(*p*-tolsal)$_2$(**CXpy**)$_2$, the anisotropic axes were anticipated to be the *z* axis (O−Co−O), and the organic spins located on the *x*−*y* plane affect the transverse anisotropy. Attempts to construct the heterospin system with organic spin at the anisotropic axis are in progress.

EXPERIMENTAL SECTION

General Procedures. Infrared spectra were recorded on a JASCO 420 FT-IR spectrometer. ^{1}H NMR spectra were measured on a Varian UNITY-400 using $CDCl_3$ as solvent and referenced to TMS. Visible spectra were recorded on a JASCO V570 spectrometer, and an NACC cryo-system LTS-22X was attached for the low-temperature measurements. The irradiation system and the samples for vis−near IR spectra measurements are described in detail in the Supporting Information (SI). Cold-spray ionization mass spectra were recorded on a JEOL JMS-T100CS spectrometer. Elemental analyses were performed at the Analytical Center of the Faculty of Science in Kyushu University.

Magnetic Measurements. The ac and dc magnetic susceptibility data were obtained on Quantum Design MPMS2 (0 ± 10 kOe) and MPMS-5S (0 ± 50 kOe) SQUID magneto/susceptometers, respectively. The irradiation system and the sample for magnetic susceptibility measurements are described in detail in the SI.

Materials. 2-Methyltetrahydrofuran and diethyl ether were distilled from sodium benzophenone ketyl. The cobalt complex Co(*p*-tolsal)$_2$ and diazo-pyridine derivatives **D1py**, **D2py**, **D3lpy**, **D3bpy**, **D4py**, and **cD5py** were prepared by the procedure reported previously.[11a]

ASSOCIATED CONTENT

Supporting Information

Experimental details, vis−NIR spectra changes, CSI mass spectra of Co(*p*-tolsal)$_2$(**DXpy**)$_2$, **X** = **1**, **2**, **3l**, and **4**, and [Co(*p*-tolsal)$_2$(py)$_2$] in solution, and supplementary magnetic data for their photoproducts. These materials are available free of charge via the Internet at http://pubs.acs.org. Full crystallographic data (CCDC No. 966174, 996590, 966175, and 966176) for [Co(*p*-tolsal)$_2$(py)$_2$], [Co(Phlsal)$_2$(py)$_2$], **D2py**, and **D3bpy** have been deposited at the Cambridge Crystallographic Database Center and are available on request from the Director, CCDC, 12 Union Road, Cambridge, CB2 1EZ, UK (fax: +44-1223-336-033; e-mail: deposit@ccdc.cam.ac.uk or http://www.ccdc.cam.ac.uk).

AUTHOR INFORMATION

Corresponding Author

*Tel: 81-92-642-6590. Fax: 81-92-642-6590. E-mail: koga@fc.phar.kyushu-u.ac.jp.

Notes

The authors declare no competing financial interest.

ACKNOWLEDGMENTS

This work was supported by Grants-in-Aid for Scientific Research (B)(2) (Nos. 17350070 and 25288038) from the Ministry of Education, Science, Sports and Culture, Japan, and by the "Nanotechnology Support Project" of the Ministry of Education, Culture, Sports, Science and Technology (MEXT), Japan.

REFERENCES

(1) (a) Gatteschi, D.; Sessoli, R.; Villain, J. *Molecular Nanomagnets*; Oxford University Press: New York, 2006. (b) Christou, G.; Gatteschi, D.; Hendrickson, D. N.; Sessoli, R. *MRS Bull.* **2000**, *25*, 66−71.

(2) (a) Martínez-Lillo, J.; Dolan, N.; Brechin, E. K. *Dalton Trans.* **2013**, 12824−12827. (b) Mitsumoto, K.; Nishikawa, H.; Newton, G. N.; Oshio, H. *Dalton Trans.* **2012**, 13601−13608. (c) Milios, C. J.; Vinslava, A.; Wood, P. A.; Parsons, S.; Wernsdorfer, W.; Christou, G.; Perlepes, S. P.; Brechin, E. K. *J. Am. Chem. Soc.* **2007**, *129*, 8−9. (d) Milios, C. J.; Vinslava, A.; Wernsdorfer, W.; Moggach, S.; Parsons, S.; Perlepes, S. P.; Christou, G.; Brechin, E. K. *J. Am. Chem. Soc.* **2007**, *129*, 2754−2755. (e) Chakov, N. E.; Lee, S.-C.; Harter, A. G.; Kuhns, P. L.; Reyes, A. P.; Hill, S. O.; Dalal, N. S.; Wernsdorfer, W.; Abboud, K. A.; Christou, G. *J. Am. Chem. Soc.* **2006**, *128*, 6975−6989. (f) Lecren, L.; Wernsdorfer, W.; Li, Y. G.; Roubeau, O.; Miyasaka, H.; Clérac, R. *J. Am. Chem. Soc.* **2005**, *127*, 11311−13117.

(3) (a) Meihaus, K. R.; Long, J. R. *J. Am. Chem. Soc.* **2013**, *135*, 17952−17957. (b) Rinehart, J. D.; Fang, M.; Evans, W. J.; Long, J. R. *Nat. Chem.* **2011**, *3*, 538−542. (c) Rinehart, J. D.; Fang, M.; Evans, W. J.; Long, J. R. *J. Am. Chem. Soc.* **2011**, *133*, 14236−14239. (d) Guo, Y.-N.; Xu, G.-F.; Wernsdorfer, W.; Ungur, L.; Guo, Y.; Tang, J. K.; Zhang, H.-J.; Chibotaru, L. F.; Powell, A. K. *J. Am. Chem. Soc.* **2011**, *133*, 11948−11951.

(4) (a) Rinck, J.; Novitchi, G.; Van den Heuvel, W.; Ungur, L.; Lan, Y. H.; Wernsdorfer, W.; Anson, C. E.; Chibotaru, L. F.; Powell, A. K. *Angew. Chem., Int. Ed.* **2010**, *49*, 7583−7587. (b) Baskar, V.; Gopal, K.; Helliwell, M.; Tuna, F.; Wernsdorfer, W.; Winpenny, R. E. P. *Dalton Trans.* **2010**, 4747−4750. (c) Osa, S.; Kido, T.; Matsumoto, N.; Re, N.; Pochaba, A.; Mrozinski, J. *J. Am. Chem. Soc.* **2004**, *126*, 420−421.

(5) (a) Jiang, S.-D.; Wang, B.-W.; Su, G.; Wang, Z.-M.; Gao, S. *Angew. Chem., Int. Ed.* **2010**, *49*, 7448−7451. (b) Lin, P.-H.; Burchell, T. J.; Ungur, L.; Chibotaru, L. F.; Wernsdorfer, W.; Murugesu, M. *Angew. Chem., Int. Ed.* **2009**, *48*, 9489−9492. (c) Pointillart, F.; Bernot, K.; Sessoli, R.; Gatteschi, D. *Chem.−Eur. J.* **2007**, *13*, 1602−1609. (d) Ishikawa, N.; Sugita, M.; Wernsdorfer, W. *J. Am. Chem. Soc.* **2005**, *127*, 3650−3651. (e) Ishikawa, N.; Sugita, M.; Ishikawa, T.; Koshihara, S.; Kaizu, Y. *J. Am. Chem. Soc.* **2003**, *125*, 8694−8695.

(6) (a) Zadrozny, J. M.; Liu, J. J.; Piro, N. A.; Chang, C. J.; Hill, S.; Long, J. R. *Chem. Commun.* **2012**, 3927−3929. (b) Jurca, T.; Farghal, A.; Lin, P.-H.; Korobkov, I.; Murugesu, M.; Richeson, D. S. *J. Am. Chem. Soc.* **2011**, *133*, 15814−15817. (c) Zadrozny, J. M.; Long, J. R. *J. Am. Chem. Soc.* **2011**, *133*, 20732−20734. (d) Harman, W. H.; Harris, T. D.; Freedman, D. E.; Fong, H.; Chang, A.; Rinehart, J. D.; Ozarowski, A.; Sougrati, M. T.; Grandjean, F.; Long, G. J.; Long, J. R.; Chang, C. J. *J. Am. Chem. Soc.* **2010**, *132*, 18115−18126. (e) Freedman, D. E.; Harman, W. H.; Harris, T. D.; Long, G. J.; Chang, C. J.; Long, J. R. *J. Am. Chem. Soc.* **2010**, *132*, 1224−1225.

(7) Abragam, A.; Bleaney, B. *Electron Paramagnetic Resonance of Transition Ions*; Clarendon Press: Oxford, 1970.

(8) (a) Zhao, H. H.; Heintz, R. A.; Dunbar, K. R.; Rogers, R. D. *J. Am. Chem. Soc.* **1996**, *115*, 12844−12845. (b) Manriquez, J. M.; Yee, G. T.; McLean, R. S.; Epstein, A. J.; Miller, J. S. *Science* **1991**, *252*, 1415−1417. (c) Caneschi, A.; Gatteschi, D.; Laugier, J.; Rey, P.; Sessoli, R. *Inorg. Chem.* **1988**, *27*, 1553−1557.

(9) (a) Murashima, K.; Watanabe, T.; Kanegawa, S.; Yoshihara, D.; Inagaki, Y.; Karasawa, S.; Koga, N. *Inorg. Chem.* **2012**, *51*, 4982−4993. (b) Karasawa, S.; Koga, N. *Inorg. Chem.* **2011**, *50*, 2055−2057. (c) Zhu, Z.; Karasawa, S.; Koga, N. *Inorg. Chem.* **2005**, *44*, 6004−6011. (d) Morikawa, H.; Imamura, F.; Tsurukami, Y.; Itoh, T.; Kumada, H.; Karasawa, S.; Koga, N.; Iwamura, H. *J. Mater. Chem.* **2001**, 493−502. (e) Karasawa, S.; Kumada, H.; Koga, N.; Iwamura, H. *J. Am. Chem. Soc.* **2001**, *123*, 9685−9686. (f) Karasawa, S.; Sano, Y.; Akita, T.; Koga, N.; Itoh, T.; Iwamura, H. *J. Am. Chem. Soc.* **1998**, *120*, 10080−10087.

(10) Jeon, I.-R.; Park, J. G.; Xiao, D. J.; Harris, T. D. *J. Am. Chem. Soc.* **2013**, *135*, 16845−16848.

(11) (a) Karasawa, S.; Nakano, K.; Tanokashira, J.; Yamamoto, N.; Yoshizaki, T.; Koga, N. *Dalton Trans.* **2012**, 13656−13667. (b) Karasawa, S.; Koga, N. *Inorg. Chem.* **2011**, *50*, 5186−5195. (c) Yoshihara, D.; Karasawa, S.; Koga, N. *Polyhedron* **2011**, *30*, 3211−3217. (d) Yoshihara, D.; Karasawa, S.; Koga, N. *J. Am. Chem. Soc.* **2008**, *130*, 10460−10461. (e) Karasawa, S.; Yoshihara, D.; Watanabe, N.; Nakano, M.; Koga, N. *Dalton Trans.* **2008**, 1418−1421. (f) Tobinaga, H.; Suehiro, M.; Itoh, T.; Zhou, G.; Karasawa, S.;

Koga, N. *Polyhedron* **2007**, *26*, 1905−1911. (g) Karasawa, S.; Zhou, G.; Morikawa, H.; Koga, N. *J. Am. Chem. Soc.* **2003**, *125*, 13676−13677. (h) Koga, N.; Karasawa, S. *Bull. Chem. Soc. Jpn.* **2005**, *78*, 1384−1400.
(12) (a) Kanegawa, S.; Karasawa, S.; Maeyama, M.; Nakano, M.; Koga, N. *J. Am. Chem. Soc.* **2008**, *130*, 3079−3094. (b) Kanegawa, S.; Karasawa, S.; Nakano, M.; Koga, N. *Bull. Chem. Soc. Jpn.* **2006**, *79*, 1372−1382. (c) Kanegawa, S.; Karasawa, S.; Nakano, M.; Koga, N. *Chem. Commun.* **2004**, 3590−3591.
(13) (a) Kuzniarska-Biernacka, I.; Bartecki, A.; Kurzak, K. *Polyhedron* **2003**, *22*, 997−1007. (b) Holland, J. M.; Kilner, C. A.; Thornton-Pett, M.; Halcrow, M. A. *Polyhedron* **2001**, *20*, 2829−2840.
(14) (a) Lever, A. B. P. *Inorganic Electronic Spectroscopy*, 2nd ed.; Elsevier Publishers: Amsterdam, 1984. (b) Cotton, F. A.; Goodgame, D. M. L.; Goodgame, D. *J. Am. Chem. Soc.* **1961**, *83*, 4690−4699.
(15) Yamanoi, Y.; Sakamono, Y.; Kusukawa, T.; Fujita, M.; Sakamoto, S.; Yamaguchi, K. *J. Am. Chem. Soc.* **2001**, *123*, 980−981.
(16) Kahn, O. *Molecular Magnetism*; Wiley-VCH Publishers: Weinheim, 1993.
(17) (a) Sarkar, M.; Aromí, G.; Cano, J.; Bertolasi, V.; Ray, D. *Chem.−Eur. J.* **2010**, *16*, 13825−13833. (b) Pardo, E.; Ruiz-García, R.; Lloret, F.; Faus, J.; Julve, M.; Journaux, Y.; Novak, M. A.; Delgado, F. S.; Ruiz-Pérez, C. *Chem.−Eur. J.* **2007**, *13*, 2054−2066. (c) Rizzi, A. C.; Brondino, C. D.; Calvo, R.; Baggio, R.; Garland, M. T.; Rapp, R. E. *Inorg. Chem.* **2003**, *42*, 4409−4416. (d) Caneschi, A.; Gatteschi, D.; Lalioti, N.; Sessoli, R.; Sorace, L.; Tangoulis, V.; Vindigni, A. *Chem.−Eur. J.* **2002**, *8*, 286−292.
(18) Shores, M. P.; Sokol, J. J.; Long, J. R. *J. Am. Chem. Soc.* **2002**, *124*, 2279−2292.
(19) (a) Miyasaka, H.; Clérac, R.; Mizushima, K.; Sugiura, K.; Yamashita, M.; Wernsdorfer, W.; Coulon, C. *Inorg. Chem.* **2003**, *42*, 8203−8213. (b) Aubin, S. M. J.; Sun, Z. M.; Pardi, L.; Krzystek, J.; Folting, K.; Brunel, L. C.; Rheingold, A. L.; Christou, G.; Hendrickson, D. N. *Inorg. Chem.* **1999**, *38*, 5329−5340.
(20) (a) Langley, S. K.; Chilton, N. F.; Moubaraki, B.; Murray, K. S. *Dalton Trans.* **2011**, 12201−12209. (b) Moushi, E. E.; Stamatatos, T. C.; Wernsdorfer, W.; Nastopoulos, V.; Christou, G.; Tasiopoulos, A. J. *Inorg. Chem.* **2009**, *48*, 5049−5051. (c) Murugesu, M.; Takahashi, S.; Wilson, A.; Abboud, K. A.; Wernsdorfer, W.; Hill, S.; Christou, G. *Inorg. Chem.* **2008**, *47*, 9459−9470. (d) Stamatatos, T. C.; Abboud, K. A.; Wernsdorfer, W.; Christou, G. *Angew. Chem., Int. Ed.* **2007**, *46*, 884−888.
(21) (a) Cole, K. S.; Cole, R. H. *J. Chem. Phys.* **1941**, *9*, 341−351. (b) Dekker, C.; Arts, A. F. M.; De Wijn, H. W.; Van Duyneveldt, A. J.; Mydosh, J. A. *Phys. Rev. B* **1989**, *40*, 11243−11251.
(22) (a) Hendrickson, D. N.; Christou, G.; Ishimoto, H.; Yoo, Y.; Brechin, E. K.; Yamaguchi, A.; Rumberger, E. M.; Aubin, S. M. J.; Sun, Z. M.; Aromi, G. *Polyhedron* **2001**, *20*, 1479−1488. (b) Thomas, L.; Caneschi, A.; Barbara, B. *Phys. Rev. Lett.* **1999**, *83*, 2398−2401.
(23) (a) Cirera, J.; Ruiz, E.; Alvarez, S.; Neese, F.; Kortus, J. *Chem.−Eur. J.* **2009**, *15*, 4078−4087. (b) Ruiz, E.; Cirera, J.; Cano, L.; Alvarez, S.; Loose, C.; Kortus, J. *Chem. Commun.* **2008**, 52−54. (c) Waldmann, O. *Inorg. Chem.* **2007**, *46*, 10035−10037.
(24) Morikawa, H.; Karasawa, S.; Koga, N. *Appl. Magn. Reson.* **2003**, *23*, 507−515.
(25) In the 1:4 complex $Co(Cl)_2(\mathbf{C1py})_4$, the exchange coupling parameter, $J_{Co\text{-}carbene}$, between the cobalt ion and the carbene was estimated to be 51 K.[11e]

dx.doi.org/10.1021/ic403074d | *Inorg. Chem.* 2014, 53, 5447−5457